Gold cluster coverage effect on H_2 production over rutile TiO_2(110)

K. Katsiev†, G. Harrison‡, Y. Al-Salik†, G. Thornton*,‡ and H. Idriss*,†

†Fundamental Catalysis, SABIC-CRD at KAUS T, Thuwal, Saudi Arabia.
‡ Department of Chemistry and London Centre for Nanotechnology, University College London, 20 Gordon Street, London WC1H 0AJ, U.K.

*Emails: idrissh@sabic.com; h.idriss@ucl.ac.uk; g.thornton@ucl.ac.uk

ABSTRACT

Unlike thermally driven catalytic reactions by metal nanoparticles, reaction rates in photo-catalysis do not scale with either the density of nanoparticles or their size. Because of the complexity of multi-component photo-catalysts in powder form, this lack of correlation, routinely observed for decades, is still not yet understood. In order to explore this phenomenon, H_2 production from ethanol over Au clusters with different coverages deposited on single crystal rutile TiO_2(110) were studied by scanning tunneling microscopy and online mass spectrometry. There is a non-linear increase of the H_2 production with increasing gold coverage. The key determining factor appears to be the Au inter-cluster distance. Increasing this distance resulted in an increase in the normalized production. These results are explained in terms of competition between clusters for excited electrons to reduce H^+ (of surface OH groups) to H_2. It was possible to determine the proportionality factor between the hydrogen production and the number of absorbed photons. A slope close to one is found, which is in line with the "current doubling effect" in electrocatalysis. Moreover, pump probe transient absorption spectroscopy measurements were conducted. Results show that excited electrons transfer from the conduction band of TiO_2 to Au particles within the first picoseconds after UV excitation. The fact that Au metal inter-cluster distances directly affect the reaction rate indicates that there is an optimum arrangement between the metal and the semiconductor that could potentially be achieved by nano-structuring.

Keywords

Gold clusters; photocatalytic hydrogen production; charge carrier diffusion length; current double effect; rutile TiO_2(110) single crystal; reaction rate.

INTRODUCTION

Considerable progress has been made in the last few years in order to improve the efficiency of photocatalytic production of hydrogen using sunlight. However, a fundamental understanding of the associated metal-support interaction is still lacking, with most of the concepts being adopted from thermally driven catalysis. In this work, we investigate the effect of Au cluster surface density on a rutile TiO_2(110) single crystal in the reaction of H_2 production from ethanol. [1-3]

Despite the large number of photocatalytic studies conducted on thin film and powder systems, [4] little intrinsic kinetic data is available. This is in large part due to the complexity of the light-matter interaction, together with the effect of semiconductor and metal particle size and crystallographic orientation as well as mass transfer within the porous supports. Photocatalytic processes typically involve photoexcitation of a semiconductor using photons with energy equal or larger than its bandgap, generating electron–hole pairs. A fraction of the created electrons and holes react with adsorbed species leading to two-electron molecular hydrogen production and four-electron molecular oxygen production. It is only this fraction that leads to catalysis; all other charge carriers recombine or are trapped in the bulk or on the surface. The process of reduction of hydrogen ions to hydrogen molecules requires a metal that can trap the photo-excited electrons from the conduction band and transfer them to hydrogen ions. The effectiveness of a photo-catalyst can be translated into its ability to utilize these electrons (and holes) efficiently, with as little as possible charge carrier recombination. Some attempts have been made to understand these processes by varying the particle size and surface density on the reaction[4-14] over supported metal powder systems. However, so far none has reported photocatalytic studies for gold on single crystal model surfaces, which have the potential to yield an atomic-level understanding.

In this context, planar model catalysts consisting of metal clusters on a single crystal support retain the critical features of most practical high surface area metal catalysts and are suitable for a broad range of surface science studies. Moreover, a well-defined planar surface has an advantage for light harvesting because of the absence of shadowing/scattering that occurs in powder systems. The catalytic activity of gold is well studied in the field of heterogeneous catalysis.[14] Gold particles, when larger than a certain *threshold* size, are catalytically less active than other transition metals. However, when Au is dispersed as nanoparticles <5 nm in diameter and supported on a metal oxide, e.g. TiO_2, it exhibits high activity for partial oxidation of hydrocarbons, low-temperature catalytic CO oxidation, hydrogenation of unsaturated hydrocarbons, reduction of nitrogen oxides, and epoxidation [15-

[29]. In this work, we focus on the role of the metal/semiconductor interface on hydrogen ion reduction. The use of a model substrate allows us to extract quantitative information regarding the reduction process in photo-catalysis using metal clusters on top of a semiconductor photocatalyst in a well defined system before and after reaction.

EXPERIMENTAL

STM and mass spectrometry measurements were performed in two interconnected UHV chambers. The analysis chamber is equipped with an Aahrus 15 HT variable temperature STM from SPECS, a sputter gun, and e-beam sample heater. The reaction chamber is a smaller custom-made chamber housing a HALO 301 residual gas analyzer (RGA) and fitted with precision leak valves for oxygen, argon, and ethanol dosing. The base pressures of the analysis and auxiliary chambers are 1 and 5 × 10^{-10} mbar, respectively. For the photoreaction measurements, the RGA was enclosed in a Pyrex shroud with an aperture (diameter = 5 mm) to enhance product detection from the sample surface (10×10 mm^2). During mass spectrometry, with or without UV illumination, the sample was positioned ca. 1 mm away from the aperture. A 300 W MAS 303 Asahi Spectra Xe lamp was used as a source of UV and visible light. The ~~filtered~~ Xenon UV light was delivered through a fiber optic cable, equipped with a focusing lens assembly. An illumination power of *ca* 10 $mWcm^{-2}$ was measured for wavelengths close to 310-400 nm. The power output on the surface of the sample can be translated into a flux of ~1.84×10^{16} photons $s^{-1}cm^{-2}$. The temperature rise during illumination was marginal, estimated to be 2-5 °C.

The rutile (110) single crystal (clear) (10×5×2 mm^3) was purchased from *Matek* and was mounted onto a Ta sample plate by spot welding using Ta stripes. The surface was prepared by cycles of Ar^+ sputtering (10-15 minute, 1 kV, 5 μA, P =$1x10^{-5}$ mbar) and annealing to ca. 1050 K until a flat contaminant-free morphology was determined by scanning tunneling microscopy (STM), at which point the crystal was deep blue. Such a surface typically contains about 5% monolayer (ML, defined with respect to Ti_{5c} sites on an ideal planar surface, this corresponds to ~5.2×10^{14} Ti atoms/cm^2) of bridging oxygen vacancies[21]. Parallel work with XPS indicates that our preparation method gives a largely oxidized surface with sharp Ti 2p lines and C contamination below 0.2 at. %. The sample temperature was monitored with a Sirius pyrometer (*Process Sensors*). The TiO_2(110) surface was deemed clean when bright rows of Ti_{5c} were visible with characteristic steps, with a unit cell of (3 × 6.5 $Å^2$) and minimal coverage of large contaminants (approximately 0.005 ML). The surface was hydroxylated (ca. 7% ML) by exposure to residual water in the UHV chamber. h-TiO_2(110) is chosen for study because of its stability and because it is representative of (110) facets of polycrystalline

materials. Au cluster growth on h-TiO_2(110) has been studied previously.[16, 23] Figures S1 and S2 give details on the extent of hydroxylation and show marginal differences in the hydroxyl density between the TiO_2(110) surface with and without Au. In-plane and height STM calibration was determined by reference to the (110) unit cell and rutile step height (3.25 Å).

The STM tip used during this study was made by electrochemical etching of a tungsten wire (0.20 cm diameter). Prior to measurements, the tip was conditioned to obtain atomic resolution images by repetitive +5 V sample bias pulses. Ethanol (99.85%) purchased from *VWR* was contained within a glass vial attached to a gas line, and dosed via back-filling the chamber through a UHV precision leak valve. The ethanol was purified by standard freeze-pump-thaw cycles and monitored by RGA. Exposures of ethanol in this work are quoted in Langmuir (L) (1 Langmuir = 1.33×10^{-6} mbar s), where the uncompensated chamber pressure was about 1×10^{-9} mbar. Other alcohols were also studied (methanol and iso-propanol); both were treated similarly to ethanol before dosing. Gold was vapor-deposited onto the substrate at room temperature in UHV from an ultrahigh purity gold wire (Goodfellow) wrapped around a resistively heated filament. Au cluster sizes were also monitored with time and no changes at RT occurred. The density of surface hydroxyls after Au deposition is given in Figure S2.

Transient absorption spectroscopy (TAS) measurements (from 0.1 ps to 3 ns timescale) are based on a regeneratively amplified Ti:sapphire laser system, which produces 800 nm laser pulses of ~100 fs pulse width at a repetition rate of 1 kHz (Coherent Inc.) driven by Excipro pump-probe spectrometer (CDP, Moscow). The energy of the pump pulses was optimized for excitation at 340 nm generated by an optical parametric amplifier (TOPAS Prime, Spectra-Physics) and a frequency mixer (NirUVis, Light conversion). The fluence of the pump power was adjusted by using neutral density (ND) filters to avoid multiple exciton generation. To generate the probe pulses (UV visible and NIR wavelength continuum, white light) another fraction of the 800 nm amplified pulses was focused onto a 2-mm thick calcium fluoride (CaF_2) crystal. Depending on the path length of the probe beam, the excited state lifetime of the species was measured up to a pump-probe delay of 3 ns. To achieve better signal to noise ratios the resulting white light was split into two channels named as probe and reference, respectively and focused on two different fiber optics. The pump pulses were overlapped on the sample with the probe pulses after passing through a synchronized chopper (500 Hz) that blocked alternate pump pulses. The change in absorption (ΔA) of the excited state are calculated by subtracting absorption of the excited and unexcited sample. A powder study was conducted over a series of Au/TiO_2 rutile nanofibers (more details on these samples can be found in ref. 5 and in Figure 3 and Table 3 of reference 18). For both powder and single crystal in situ TAS

studies, the N_2 used to purge the reactor (cell) was 99.999 %; based on GC measurements the threshold is found to be 0.3 vol. %. In the case of liquid/solid reactions, the aqueous solution was at neutral pH. Transmission Electron Microscopy measurements were conducted at the University of St. Andrews by Dr Wuzong Zhou (Department of Chemistry), using a Jeol 2011 HRTEM operated at an accelerating voltage of 200 kV.

RESULTS AND DISCUSSION

A. Scanning Tunneling Microscopy

The clean rutile TiO_2(110) sample reveals a (1×1) surface termination, with terraces of *ca.* 100 Å size (Figure 1A). Bright rows with a separation of 3 Å, running in the [001] direction, are displayed in the inset, represent Ti_{5c}^{4+} ions. Bridging oxygen atoms (O_{br}) are located in between the bright rows, while bridging hydroxyls (OH_{br}) are the brighter features in similar positions at an apparent height of ~0.8 Å. Au deposited onto the surface of a clean rutile TiO_2(110) surface was studied at room temperature at five different coverages in the dark before exposure to ethanol. The STM images are shown in Figure S3, with the cluster size distributions in Figure S4. Example STM images of Au supported on TiO_2(110) are shown in Figure 1B, C. In line with earlier work [14,19-28] sub-nanometer diameter hemispherical features are observed situated at the upper step edge sites, where the diameter is taken as twice the STM height. The hemispherical features are identified as Au clusters formed by the surface diffusion and nucleation at room temperature (more details on the methodology used to determine the cluster sizes are given in Figure S5).

The Au/TiO_2(110) surface was exposed to ethanol (13.5 L) and a coverage of ~0.3 ML was determined using STM. The corresponding images are presented in Figure 1E, where features of 6 Å diameter are present. This is consistent with previously recorded STM images of ethanol molecules on rutile TiO_2(110).[29,30] Figure S3 shows no change in the Au clusters size upon ethanol adsorption.

B. Online Mass Spectrometry

Online mass spectrometry experiments were conducted in order to study the photocatalytic products. The ethanol covered Au/TiO_2(110) surface was exposed to UV light in UHV ~10^{-9} mbar, while monitoring the m/e 2 QMS signal. The QMS signals from other products, that is methyl radicals (m/e 15), acetaldehyde (m/e 29), and CO_2 (m/e 44 – that includes contribution from the parent mass of acetaldehyde) are presented in the supplementary information (Figure S6). A sharp rise followed by a decay was observed for all products. In an identical experiment using deuterated ethanol (6d-ethanol) (see Figure S7), the observation of m/e 4 (attributed to D_2) and m/e 3 (attributed to HD) signals allowed us to assign the m/e 2 as

molecular hydrogen formed from the photo-decomposition of CH_3CH_2OH and formation of H_2 from surface hydroxyls. In a separate set of experiments, we have exposed the clean surface to D_2O (repeated cycles of 1 x 10^{-7} mbar at 300 K) then dosed non-deuterated ethanol. While most of the signal was m/e 2, a small fraction of about 1% of D_2 (m/e 4) was observed. The photo-reforming of alcohols has been studied in some detail on polycrystalline[9, 17, 22, 31, 32, 33] and single crystal[34-38] TiO_2 surfaces by many groups. The reaction products observed are dependent on the experimental environment. For instance, in an aqueous environment, the reaction in Equation 1 will prevail and differences in observed reaction products may be traced back to mass transfer and solubility parameters. In a solid-gas system, water partial pressure is the key parameter determining the reaction products.

The product distribution observed in our solid-gas experiments can be explained by a series of reactions. First, the overall reaction involves 12 electrons:

$$CH_3CH_2OH + 3\,H_2O \rightarrow 12\,e^- + 12\,H^+ + 2\,CO_2 \rightarrow 6\,H_2 + 2\,CO_2 \quad \Delta G^o = -97.4\ kJ\ mol^{-1}$$

Equation 1.

Hydrogen production does not occur in the absence of the alcohol (the hole scavenger); in other words all 12 electrons originate from ethanol as per Equation 1.

The above reaction is the complete catalytic reaction that is favored thermodynamically (- ΔG) and occurs when the ratio of water to ethanol is three or above.

This reaction is the sum of three sets of reactions. The first set is the following:

$$CH_3CH_2OH + \mathbf{Ti}_{5c}\text{-}\mathbf{O}_{br} \rightarrow CH_3CH_2O\text{-}\mathbf{Ti}_{5c} + \mathbf{O}_{br}H$$ Equation 2a

Then upon photon excitation

$$CH_3CH_2O\text{-}\mathbf{Ti}_{5c} + \mathbf{O}_{br} + x\,h^+ \rightarrow CH_3CHO(g) + + \mathbf{Ti}_{5c} + \mathbf{O}_{br}H + 2\,e^-$$ Equation 2b

$$2\,O_{br}H + 2\,e^- \rightarrow H_2(g) + \mathbf{O}_{br}$$ Equation 2c

Ti_{5c} and O_{br} are nominally $Ti^{4+}{}_{5c}$ and $O^{2-}{}_{br}$ (removed from the equations for simplicity)

Where g stands for gas phase, O_{br} for bridging surface oxygen anions, Ti_{5c} for Ti cations five-fold-coordinated to oxygen anions and *h* for hole.

Equation 2a is also exothermic (the adsorption energy of ethanol on TiO_2(110) is about 1 eV).[38] Equation 2b, however, occurs upon the creation of e-h pairs after photon excitation (the *x* in

equation 2b is either 1 or 2 in the case of TiO_2, discussed in more detail in section D below). It involves the injection of two electrons from ethanol into excited TiO_2; these are transferred to the two hydrogen ions (the $O_{br}H$ of Equations 2a and 2b); equation 2c. This reaction is endothermic (ΔH: +110 kJ mol^{-1}), requiring light to excite the semiconductor or alternatively heat as in the case of CeO_2, for example[39].

The remaining two sets of reactions involve the reforming of acetaldehyde (Equation 3) and the water gas shift reaction (Equation 4). Both are presented below as a reaction network and not by their mechanistic steps. More details about both can be found elsewhere[31, 32]. Part of acetaldehyde before desorption in the gas phase (Equation 2b) can further react to CO and H_2 (reforming of acetaldehyde)

$$CH_3CHO(a) + H_2O \rightarrow 2\,CO(a) + 3H_2 \qquad \text{Equation 3}$$

Adsorbed CO would then further react with water to give CO_2 and H_2 (water gas shift reaction)

$$2\,CO + 2\,H_2O \rightarrow 2\,CO_2 + 2\,H_2 \qquad \text{Equation 4}$$

The sum of equations 2, 3 and 4 gives equation 1.

In the set of experiments conducted in this work, where the hydroxylated surface (of about 7%) is pre-dosed with ethanol then exposed to UV light, the main reaction is that of equation 2. Presented in Figures S8-S10 are the reaction products from ethanol (as well as two other alcohols for comparison: methanol and i-propanol); also presented are the mass spectrometry correction factors. Inspection of the signal of m/e 2 (hydrogen) and m/e 29 (-CHO of the aldehyde) in the case of methanol and ethanol indicates a ratio very close to one. This indicates that equation 2 dominates. This is expected as most of the acetaldehyde (formaldehyde) formed would desorb and therefore the contribution of reactions 3 and 4 would be minor. The case of i-propanol (a secondary alcohol) is more complex, and is not treated further in this work.

The main point, however, is that the electrons needed to reduce hydrogen ions are provided from ethanol and therefore the origin of hydrogen ions (surface hydroxylation prior to ethanol adsorption or surface hydroxylation due to the dissociative adsorption of ethanol) does not affect the reaction yield: for each hydrogen molecule two electrons are provided by ethanol).

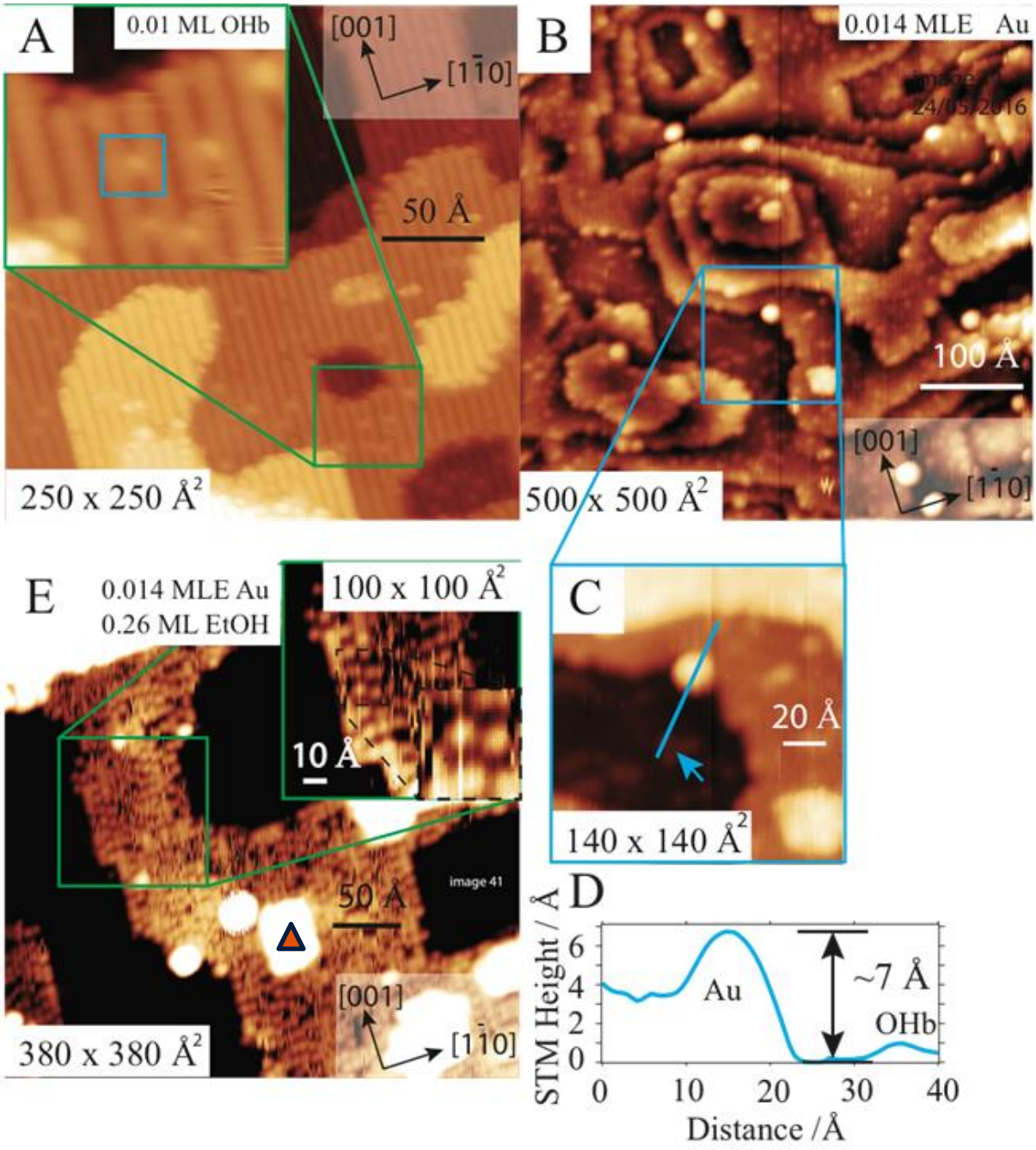

Figure 1.

STM images of a clean TiO_2(110) and Au/TiO_2(110) rutile single crystal.
(A) Large area image of clean rutile TiO_2(110) (250 × 250 Å^2, inset: an enlarged image (52 × 52 Å^2), where an OH_{br} is identified.
(B) Large area image of Au/TiO_2(110) (500 × 500 Å^2, +2.1 V, 0.04 nA).
(C) A high-resolution image (140 × 140 Å^2), a blue height profile is indicated.
(D) A line height profile of the Au cluster of 5 Å height.
(E) A large-scale image of an 0.29 ML ethanol/Au/TiO_2(110) image (380 × 380 Å^2, 1.48 V, 0.08 nA) inset: an enlarged image (95 × 95 Å^2). The rectangular shape labeled with a triangle is a small terrace and the two circular structures on its left are those of Au clusters with FWHM of 9-10 Å and height of 6-8 Å (more details are given in Figure S11C).
More images related to these surfaces can be found in Figures S3, S5 and S11.

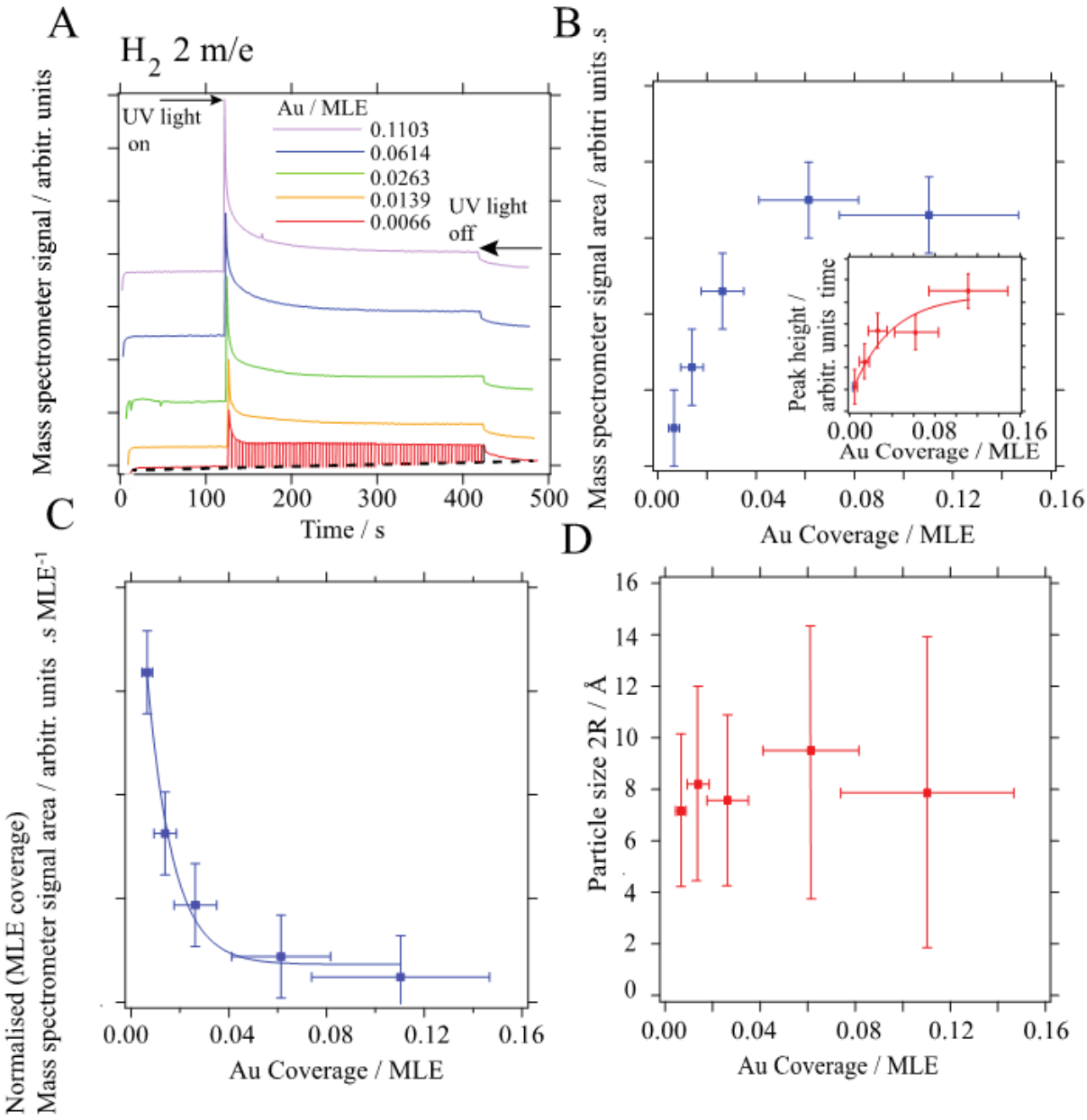

Figure 2.

Mass spectrometry spectra recorded over ethanol/Au/TiO_2(110) rutile single crystal:

(A) 300 K on-line mass spectrometry of m/e 2 after exposure of ethanol/Au-rutile TiO_2(110) single crystal to UV light in UHV. The black dashed line and vertical red lines for 0.0066 MLE of Au indicate the baseline and area of spectra integral.
(B) A plot of the integrated spectra using a horizontal baseline defined in (**A)** of the m/e 2 as a function of Au coverage. Inset: the QMS ion current peak height of the spectra in (**A**).
(C) Peak areas shown in **(B)**, normalized to Au coverage (in monolayer equivalents).
(**D**) The cluster size in 2R/Å as a function of Au coverage, where R is the STM height averaged over 60-140 clusters.
The number of clusters counted is as follow:
5 minutes evaporation: 48 clusters, two STM images. Total area = 5000 nm^2
10 minutes evaporation: 112 clusters, two STM images. Total area = 7500 nm^2

20 minutes evaporation: 148 clusters, two STM images. Total area = 5000 nm^2
35 minutes evaporation: 150 clusters, two STM images. Total area = 5000 nm^2
60 minutes evaporation: 137 clusters, one STM image. Total area = 2028 nm^2

One important observation during the online mass spectrometry experiments was the need for surface activation. This consisted of first exposing the ethanol-covered surface to UV light in the same conditions as for the actual data collection. This was noticed during data collection, where the first set of results always showed less activity than the subsequent ones. The exact role of this "activation" in the enhancement of the performance is not known. However, it resonates well with the induction period that is frequently observed in photoreactions on powder photocatalytic systems.[7] It is thought to arise from further cleaning of the surface from adventitious molecular and/or oxygen atoms on Au clusters. After this activation, the Au/TiO_2 (110) was active for the many cycles needed for the study without signs of deactivation within experimental errors of about 10%.

The surface of ethanol covered Au/TiO_2(110) after photoreaction was examined by STM routinely (supplementary Figure S11). It was found to be almost fully depleted of non-Au adsorbates, with a small concentration of OH_{br}. The cluster sizes of Au showed small changes as shown in Figure S11, where the average size increased to 12Å. It is also important to mention that in the absence of Au, no reaction took place in UHV upon exposing an ethanol covered TiO_2(110) to UV light. Previous work by us has shown that as-prepared TiO_2 rutile and anatase single crystals are active for the photo-catalytic decomposition of ethanol in UHV when molecular oxygen is present to act as an electron trap[30,40] . Other studies have shown the photo-catalytic activity of TiO_2 single crystals in a water/methanol mixture[41,42]. Fresh ethanol covered Au/TiO_2(110) surfaces were prepared with a range of Au coverage from 0.006-0.11 monolayer equivalents (1 MLE is the ML coverage assuming a uniform distribution of Au atoms over the surface) and the UV light exposure was repeated. Each of the experiments was done separately and the surface was imaged with STM before dosing ethanol, after dosing ethanol as well as after the photoreaction (in some runs). The m/e 2 traces recorded are presented in Figure 2A. An increase in the H_2 generation with increasing Au coverage is observed. An integration of the signal was performed and displayed in Figure 2B. It is clear that the amount of molecular H_2 displays a non-linear increase with Au MLE coverage, with saturation of the signal at about 0.06 Au MLE.

C. Normalization of the reaction rate

When H_2 production is normalized to the MLE coverage of Au (proportional to the total

Au atom number), a decaying exponential (Figure 2C) is found. As the MLE coverage increases, several interconnected characteristics of the Au/rutile TiO_2(110) system change;

i) The average size (diameter) of the Au cluster changes slightly (see supplementary information Figure S4) and 2D with increasing exposure; although at the highest coverage (60 minutes) there is a tendency for the formation of a few clusters with large size (Oswald ripening) but at the same an increase in the density of much smaller particles (most likely in the form of trimers – figure S4 histogram E).

ii) More Au clusters are present on the inner terrace as opposed to the step edge,

iii) The average separation between Au clusters decreases from ~57 Å at low coverage to ~21 Å at high coverage;

It is clear that the Au cluster coverage is a decisive factor in H_2 production. The cluster number density increases monotonically in the coverage range 0.006-0.11 MLE, corresponding to a range between 9.8×10^{11} nano cluster cm^{-2} and 7.5×10^{13} nano cluster cm^{-2}. From the average cluster radii at each coverage, the surface areas were obtained assuming a hemispherical cluster shape (as detailed in Figure S5). A linear increase in cluster surface area with respect to MLE coverage is observed (Table S1); H_2 production is not proportional to the area.

In seeking an explanation for the H_2 yield dependence on Au coverage, the effect of Au on the lifetime of photo-yield charge carriers seems a likely candidate. The lifetime is modified because Au particles act as sinks for excited electrons, a phenomenon that has been evidenced by time resolved spectroscopy[43,44] and EPR measurements.[45,46] In the process of hydrogen ion reduction to molecular hydrogen two electrons are needed. These two electrons need to be situated on the same metal particle or more precisely at the interface of the same metal-semiconductor particle. This reduction process is orders of magnitude slower than the electron-hole recombination rate[31,32]. Therefore, the presence of two gold clusters within the Debye length of electron diffusion would result in a decrease of electron flow into a given metal cluster, which in turn would result in a decrease in the overall reaction production when normalized to the number of metal clusters. This is different from the situation for thermal catalytic reactions, where the reaction rate scales with the number of metal sites as long as it is not sensitive to a particular crystallographic orientation or particle size. This difference in behavior arises from the time scales of the two processes, with the “time-configuration” becoming a determining parameter in reaction rate beyond its strictly “chemical kinetic” effect. The average minimum separation between Au clusters was determined and ranged from 57 Å

at 0.0066 MLE to 21 Å at 0.11 MLE. When the H_2 signal is normalized to cluster density and plotted against inter-cluster distance, an inverse-direct linear relationship is observed (see Figure 3).

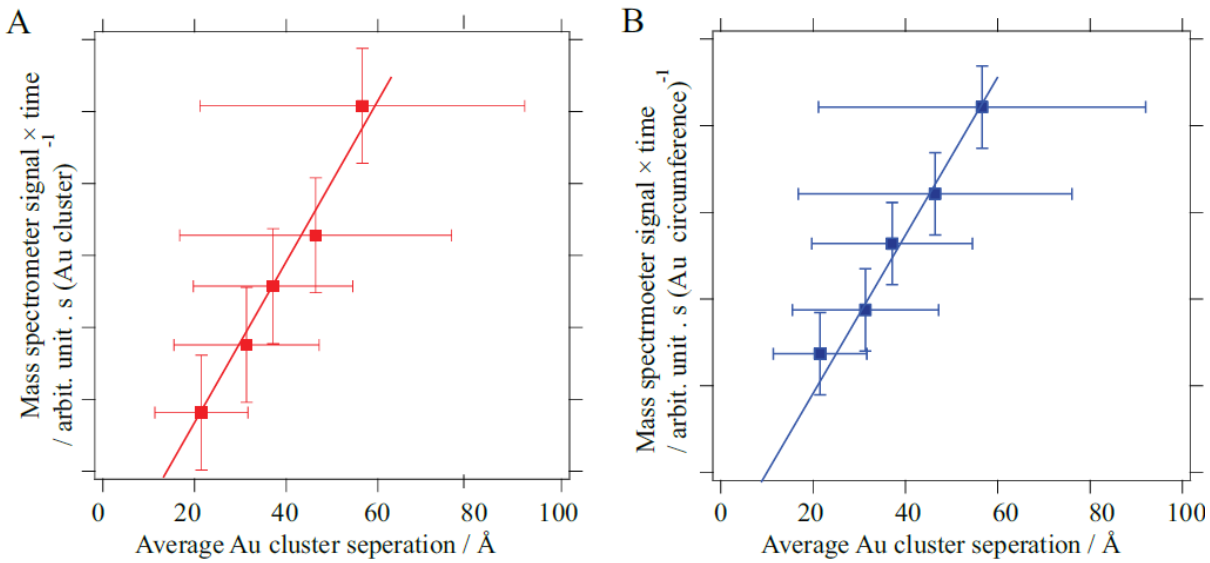

Figure 3.

(A) Normalized hydrogen production per metal cluster number as a function of the inter-cluster distance.

(B) Normalized hydrogen production per metal cluster circumference as a function of the inter-cluster distance.

The number of clusters at each coverage is given in the caption of Figure 2.

D. Effect of Photon flux

The effect of photon flux on hydrogen production is shown in Figure 4A. Integration of the hydrogen signal as a function of photon flux gives the relative hydrogen photo-yield at a given photon exposure (Figure 4B). Light scattering effects may be neglected because of the very small amount of gold. The ethanol coverage was constant. The initial part of the Figure extending from about 10^{15} to 10^{16} photons/cm^2 appears to show a linear dependence of hydrogen production and photon flux. After about 1×10^{16} photons/cm^2 s the production nearly saturates. This is mostly because all surface ethoxides have reacted (the ratio of photons to ethoxide at this flux is > 50). Irrespective of the efficiency of the system, one can correlate the number of photons used to the amount of molecular hydrogen produced. Because of the nature of the experiments (single crystal surface; no inter- or intra-particle pores), all incident photons generate a proportional number of excited electrons that are poised to directly contribute to the reaction. The slope of the line thus indicates the number of photons used per number of hydrogen molecules. The slope is found to be close to unity.

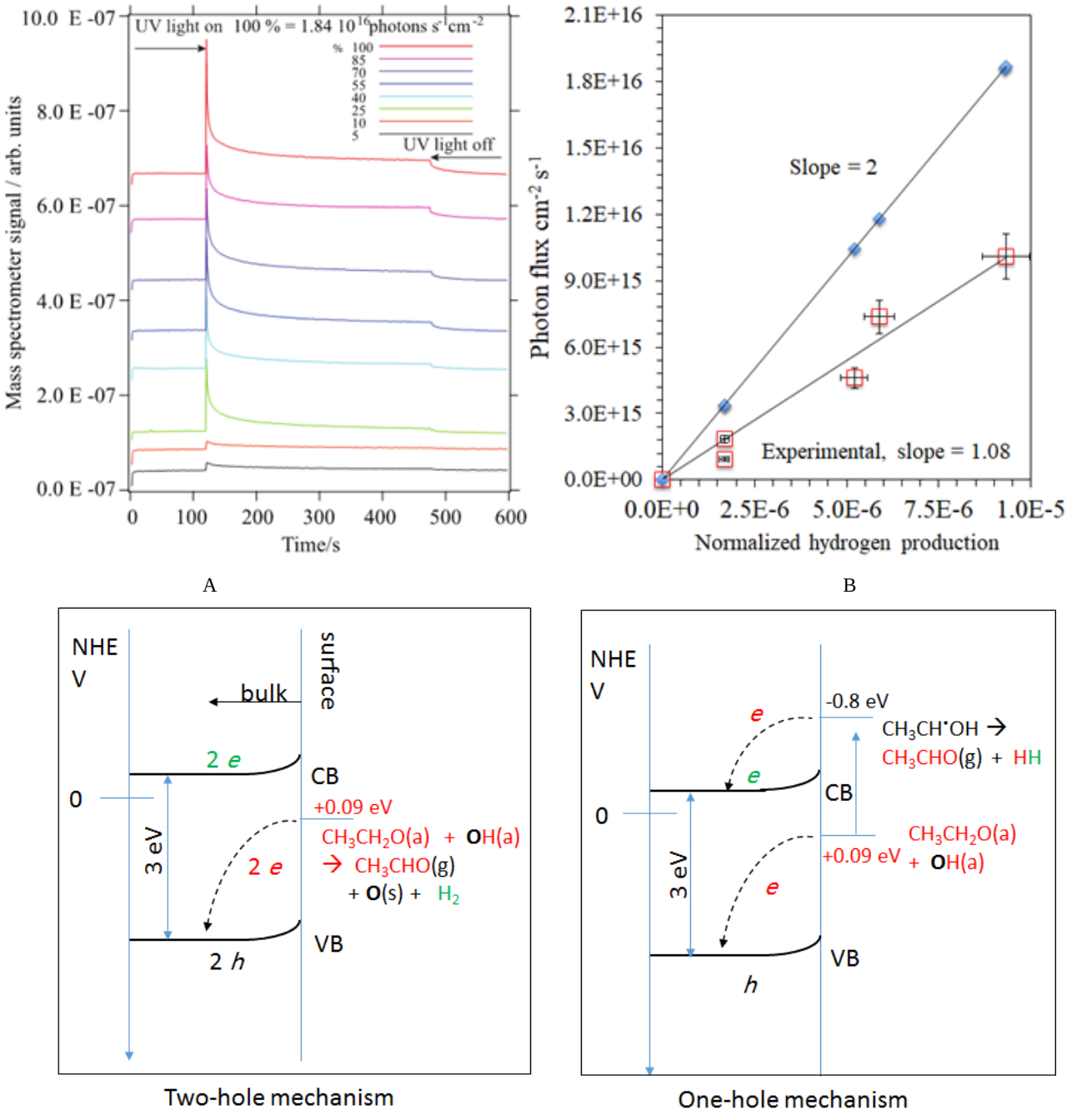

Figure 4.

Hydrogen production upon UV excitation at the indicated light flux of an ethanol saturated Au-rutile TiO_2(110) at 300 K. The Au coverage is 0.06 MLE, the average cluster size is 7.2 Å and a cluster density of 3×10^{12} clusters cm^{-2}.

(**A**) H_2 m/e 2 signal at different UV light flux; 100% = 1.84×10^{16} photons $s^{-1}cm^{-2}$.

(**B**) A plot of H_2 m/e area verses UV light flux. Also shown is the expected production if one photon or two photons per molecular hydrogen are needed (slope = 1 or slope = 2). Experimentally, the slope if found to be equal 1.29. The saturation of hydrogen production might be due to a change in reaction mechanism with photon-flux, it can also be due to depletion of surface reactants.

(**C**) A schematic representation of two-hole and one-hole mechanism. The former requires two photons for one hydrogen atom and the latter require one photon for one hydrogen molecule (the so-called "current doubling effect"). The redox potential of the radical

$CH_3C^{\bullet}HOH$ is from ref. 32. O(s): s stands for surface. Equations related to one- and two-hole mechanism are presented in Supplementary information (text 1).
Number of clusters counted:
Before UV light exposure 81 clusters, one STM image. Total area = 2500 nm^2
After UV light exposure 61 clusters, one STM image. Total area = 2500 nm^2

Since the formation of a hydrogen molecule requires two electrons, it is thus clear that the second electron originates from ethanol/ethoxide directly. This is the so called "current doubling" effect previously evidenced for methanol photo-electrochemistry over Pt/TiO_2 and ZnO[47,48] powder and (for ethanol) theoretically by DFT computation for a TiO_2(110) rutile single crystal[49]. In other words, upon one photon absorption and generation of an e-h pair, ethanol/ethoxide species inject one electron into the valence band to be trapped by a photo-yield hole. The radical formed has enough energy to transfer another electron into the conduction band of TiO_2. Both electrons in the conduction band are then used to reduce two hydrogen ions to molecular hydrogen (Figure 4C). To our knowledge, this is the first time a direct quantitative measurement of the quantum yield of hydrogen by photocatalysis has been made. It is customary when calculating the quantum yield of H_2 from alcohol photo-catalysis to assume that two photons are needed for each H_2 molecule. In other words, the QY of the reaction is often calculated by multiplying the hydrogen production by two. Results of this work give evidence that the ratio is one photon to one hydrogen molecule, which means that the often-reported quantum yields need to be halved at least in the case of TiO_2. As for the amount of H_2 produced in this work, this saturates at about 7×10^{15} photons cm^{-2} s^{-1}. The ethanol coverage is about 0.25 ML so the number of ethanol/ethoxides per cm^2 is about 1.3×10^{14} and the quantum yield of the reaction is about 2 %.

Pump probe Transient Absorption Spectroscopy (TAS)

To investigate the relationship between the Au cluster separation and charge carrier lifetime, pump probe Transient Absorption Spectroscopy (TAS) measurements were conducted. Before studying the effect of Au loading we have conducted a set of experiments on the clean TiO_2(110) rutile single crystal in the presence and absence of gas phase ethanol. The crystal was cleaned ex-situ then put into a quartz reactor, inside the pump probe equipment. Measurements of the life time decay of the clean surface were conducted in pure N_2 while those in the presence of ethanol were conducted upon introduction of a drop of ethanol inside the reactor to allow gas phase (vapor pressure ca. 10 mTorr at room temperature) to adsorb. Figure 5 presents the signal in ΔA as a function of the delay time. The delay signal is identical to what has been reported by us on a similar TiO_2(110) rutile single crystal previously[50]; in which its details were discussed.

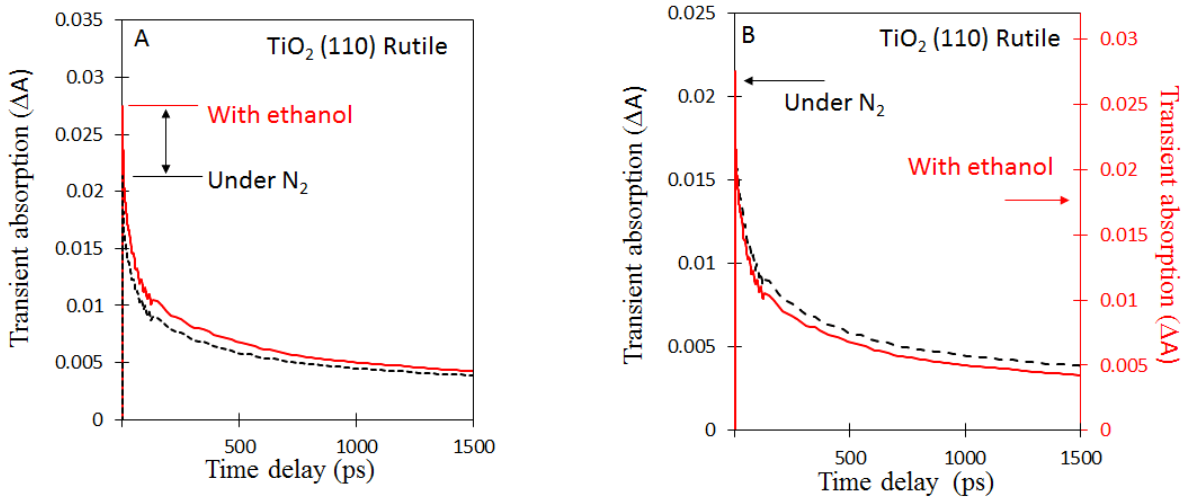

Figure 5.

Pump-probe femto second transient absorption spectroscopy of the signal at 830 nm from a clean rutile TiO_2(110) single crystal before, in inert (N_2), and after the introduction of gas phase ethanol (ca. 10mTorr in N_2), at room temperature. Excitation wavelength: 340 nm. Laser power on the sample is about 5 mW. The left side figure presents the as recorded signal while the right side presents the normalized one. A three exponential fit best described the decay ($y = y_o + A_1 \exp(-x/t_1) + A_2 \exp(-x/t_2) + A_3 \exp(-x/t_3)$)

In brief, the main signature occurs in the 800-950nm region, which is characterized by multiple peaks with exact decay time. In this work, we have monitored the decay at 830nm; the decay of other signals in the same region gives the same time constants. The signal consists of a sharp decay followed by a shallow one. This is a signature of the rutile single crystal where a fast decay is attributed to surface and near surface traps of excited electrons from the conduction band, first-order Shockley−Read−Hall-mediated, in addition to third-body Auger recombination depending on the degree of bulk reduction[50]. In the presence of ethanol, a considerable increase of ΔA is seen. This is attributed to increase in the excited electrons concentration due to retarding of the recombination process provoked by hole consumption in the presence of adsorbed ethanol. There is also a slight decrease in the lifetime of the signal (where t_2 decreased from 38 to 30 ps; t_1 and t_3 remained unchanged within standard errors)). This has been seen by others in the case of methanol on TiO_2 powder[51] and postulated to be due to the overlap of signatures from holes in the same region. In other words the signal in the 800-950nm region is not exclusive due to excited electrons trapped at about 1.5 eV below the conduction band but also to some hole signatures[51]. Next, we focus on the effect of Au clusters on the decay signal of the support. However, because of the low surface to bulk ratio of the single crystal the effect of Au is expected to be weak. Therefore, we have conducted

experiments, in addition to those on Au/TiO_2(110) single crystal, on Au particles supported on rutile nanofiber for comparison. These are elongated 100 nm wires of 20 nm width, with a BET surface area of about 100 m^2/g and loaded with a 2 wt. % Au (this catalyst has been studied in detail in references 5 and 18). Figure 6A presents XPS Au 4f of gold deposited on a clean oxidized TiO_2(110) rutile single crystal together with the Ti2p before and after Au deposition (5 minutes). Au was deposited following the same method used for STM with a similar coverage. XPS Au 4f region presents the expected shift to higher binding energy (when compared to bulk Au at 84.0 eV) due to cluster size effect[52-55]. The study was conducted after exciting TiO_2 with a 340 nm femto second laser, and probing in the 750-950 nm region. The signal is shown to decay faster in the Au/TiO_2(110) when compared to TiO_2(110) alone. As mentioned above because a large fraction of the signal originates from the bulk the effect of Au is very weak. We observe a similar trend albeit more pronounced when Au is deposited on TiO_2 rutile nanofiber. For 8 wt. % Au because the decay was very fast, a single exponential decay best fitted the signal; with t = 0.25 ps which is within the resolution of the measurements. It is thus clear that like Pt on TiO_2 [43] and Pd on C_3N_4 [56] the presence of Au clusters/particles results in decreasing the lifetime of excited electrons most likely by pumping them away due to its high work function when compared to TiO_2.

A

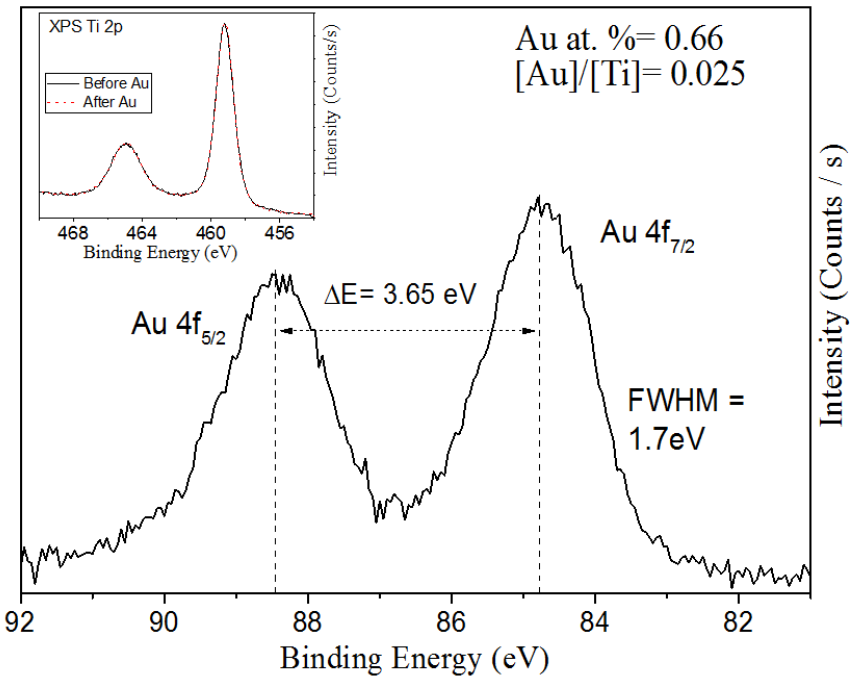

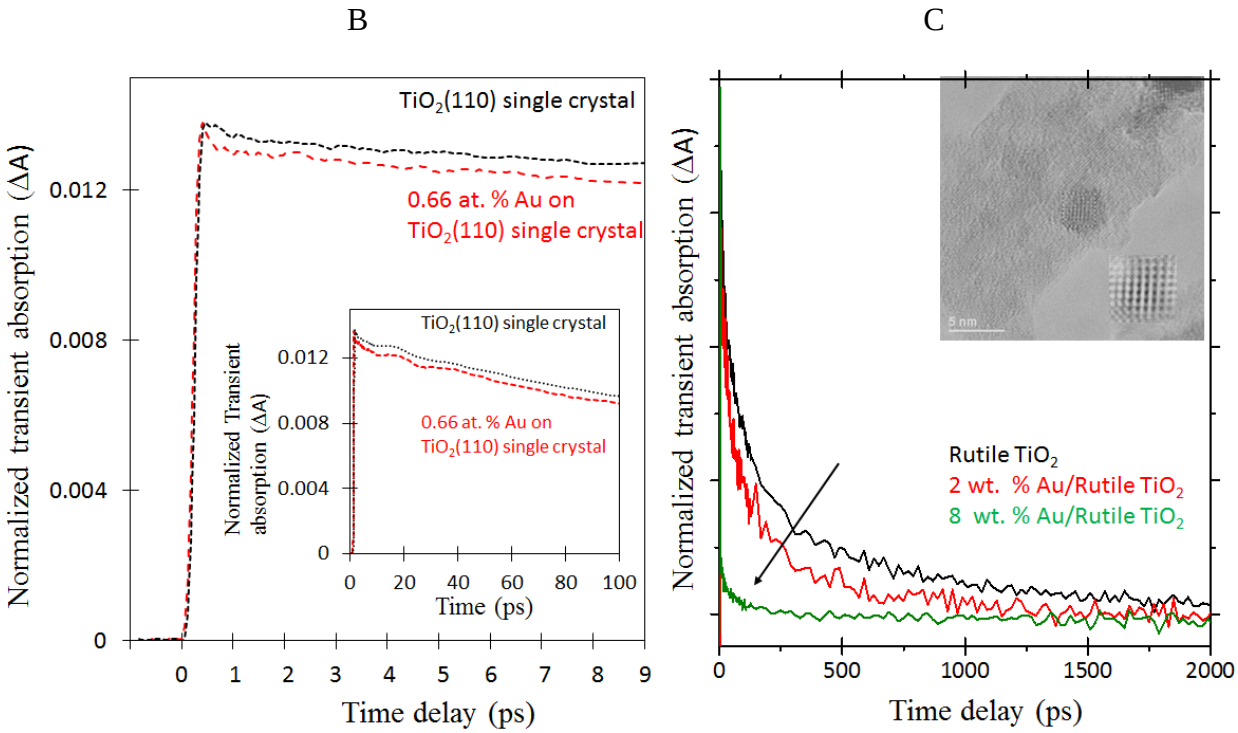

Figure 6.

A. XPS Ti 2p (inset) of clean TiO_2(110) rutile single crystal before and after Au deposition. The shift in the XPS Au4f binding energy from 84.0 eV is due to cluster size effect. The computed Au content on the surface was found to be 0.66 %. B. Pump-probe femto second transient absorption spectroscopy of a normalized signal at 830 nm from a clean rutile TiO_2(110) single crystal and of the 0.66 at. % Au/TiO_2(110) rutile single crystal, in air. Data in the inset are four-point smoothed. C. Pump-probe femto second transient absorption spectroscopy of a normalized signal at 830 nm of TiO_2 rutile nanofiber, 2 wt. Au/TiO_2 rutile and 8 wt.% Au/TiO_2 nanofiber in air. The inset in C presents a HRTEM image of a Au particle on top of the rutile TiO_2 support. Excitation wavelength: 340 nm. Laser power on the samples is about 5 mW. The time constant values are within 150 fs resolution and with reproducibility errors of 7 to 10 %. The decay for all but the 8 wt.% Au/TiO_2 is fitted with three exponential function as in figure 5. Because of the very fast decay in the case of the 8 wt.% Au/TiO_2 a single exponential function ($y= y_o + A \exp(-x/t)$)was used for up to 20ps, after which the signal has largely disappeared; t = 0.25 ps).

Figure S12 presents the diffusion length, L_D, as a function of electron mobility at two different lifetimes. Based on mass spectrometry and STM results where it appears to be an inverse relationship between Au cluster separation and reaction rate and the fact that the presence of the latter decreases excited electron lifetime it is natural to link these observations to the diffusion length of excited electrons. The exact electron mobility, μ, in TiO_2 (110) rutile single crystal may not be known because it changes with the degree of bulk reduction. Yet,

because of the square root dependency between L_D and μ, L_D changes slightly at higher mobility ($> 10^{-4}$ m^2 V^{-1} s^{-1}) so the analysis is plausibly more relevant at this mobility range and above. In addition, based on the results in Figure 4 it seems that to increase the efficiency of the reaction per cluster, one needs to have a separation of approximately 50 Å or more. The results thus combined tend to indicate that competition for excited electrons by the Au clusters decreases H_2 production (Scheme 1). That is because each metal cluster needs at least two electrons to reduce two hydrogen ions (from surface hydroxyls), in particular when considering that charge transfer for this reaction is many orders of magnitudes slower[57] than the kinetics of electron transfer from the CB of TiO_2 to Au clusters.

As mentioned in the introduction section, previous work has shown a narrow range of noble-metal cluster size and coverage on a semiconductor is required for maximum catalytic activity[4, 10, 17]. Studies of polycrystalline and nano-structured catalysts have invoked the following as plausible reasons for the variation of reaction rate with the noble metal distribution. First, the available area of semiconductor exposed to light[10, 11], secondly the number of defects created at the metal/semiconductor interface[10, 12] and finally competition between excited carriers[13]. Our results suggest that light shielding is unlikely to play a key role. This is based on the results presented in Figure 2, which evidence an exponential decay of the normalized production with a small increase of the Au coverage. STM images of bare TiO_2(110) and Au/TiO_2(110) show no obvious difference in the degree of surface hydroxylation (Figure S2). This points to a similar surface defect density following Au cluster deposition, although work by others[60] on Pt/TiO_2(110) has indicated that the presence of Pt facilitates the O-H bond dissociation of methanol. Yet, as noted above, our single crystal results point out that the most obvious effect is the inter-cluster distance. This factor was also suggested in a study of Pt/CdS[13], although in this case the critical distance between Pt clusters was identified with the spatial extent of the electronic wave functions. This observation might be more general as others have seen similar effect for the oxygen reduction reaction on Pt[61].

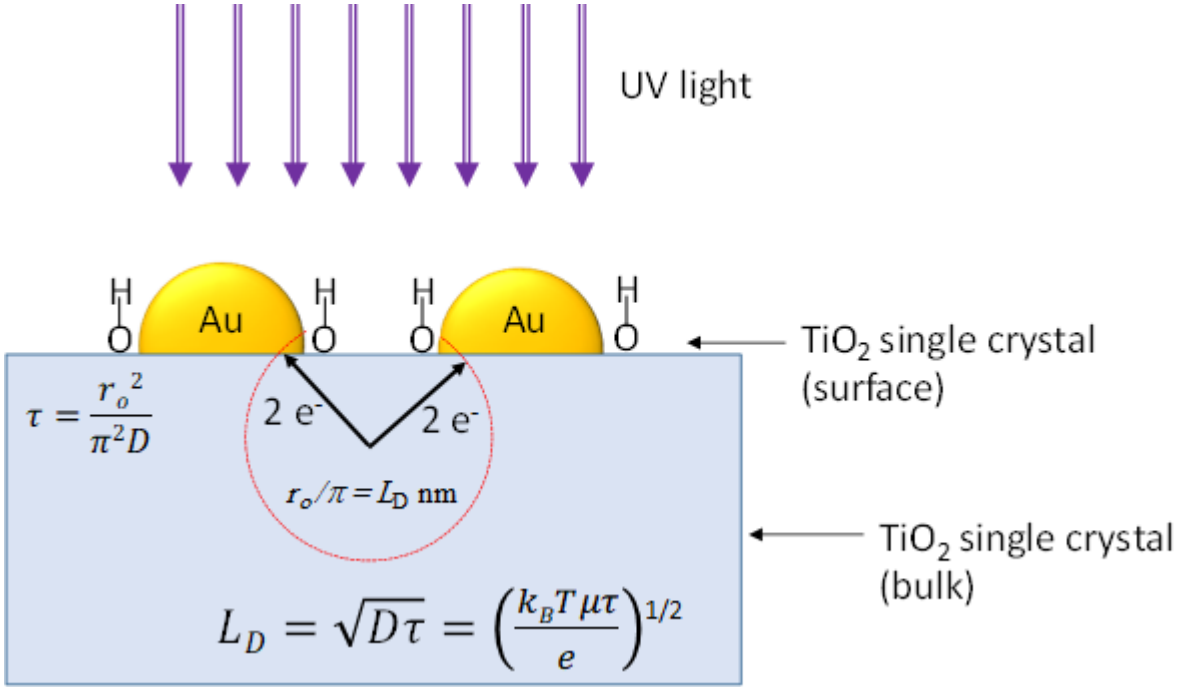

Scheme 1.

Schematic representation of the electron transfer from the conduction band of TiO_2 to Au clusters upon UV excitation. The effect of the lifetime of excited electrons on the diffusion length at different electron motilities is given in Figure S12. Based on TAS measurements, hydrogen production, and cluster separation it is postulated that the critical factor in the enhancement is the inter-cluster distance of gold clusters on the surface of the semiconductor rutile TiO_2. L_d: diffusion length, D: diffusion coefficient, τ: time constant, m: electron mobility, e: electron charge, k_B: Boltzmann constant, T: temperature, r_o: cluster radius. The effect of gold clusters on band bending of TiO_2, studied elsewhere[58, 59], is not considered in the scheme.

Conclusions

Photo-catalytic hydrogen production from ethanol over Au clusters on TiO_2(110) with sizes between 7 and 12 Å were studied using scanning tunneling microscopy (STM) and online mass spectrometry and complemented by pump-probe Transient Absorption Spectroscopy. Unlike thermal catalytic reactions, a non-linear dependence of the production with increasing gold coverage is observed. Instead, the production correlates with the separation between clusters. Femtosecond pump-probe experiments over Au/TiO_2 single crystal and powder indicate a decrease in the lifetime of excited electrons due to charge trapping by Au clusters/particles. Because molecular hydrogen production requires two electrons, increasing the cluster density within the Debye length results in competitive trapping, which in turn decreases the reaction

yield per cluster. The computed Debye length of up to 50 Å for this phenomenon further explains why Au clusters need to be dispersed more than this distance to maximize their efficiency. Hence, this result explains the reason for the deviation from linearity in photo-catalysis. Moreover, quantitative flux dependence experiments indicate that one photon is needed for one molecular hydrogen to be produced in line with the so-called "current doubling effect". In other words, the reaction quantum yield for hydrogen production using alcohols does not need to be multiplied by two as it is in practice at present. The fact that metal inter-cluster distances have such a dramatic effect on the production indicates that nanostructured synthesis is most likely the method of choice to optimize photocatalytic performance for future technologies.

Supporting information

S1. Effect of residence time on the surface hydroxylation; S2. Surface hydroxyls density; S3. STM of Au clusters deposited at RT at different deposition time; S4. Height histograms of the Au clusters; S5. The model adopted to determine the clusters height; S6. On-line mass spectrometry of desorbed products from ethanol; S7. Ethanol and deuterated ethanol photoreaction over Au/TiO_2 (110); S8. Photo-catalytic hydrogen production from ethanol, i-propanol, and methanol; S9. Photo-catalytic production of methyl radical (m/e 15), -CHO fragment, m/e 29, and CO_2 m/e 44; S10. Products desorbing during the photocatalytic reaction of i-propanol. S11. STM of Au/TiO_2(110) before (**A**) and after (**B**) UV excitation; S12. Change of diffusion length as a function of electron mobility. Table S1. Monolayer equivalent (MLE) coverage of Au, surface area cluster density, and hydrogen production. Table S2. Example of calculation. Supplementary text 1. Method of calculation of the apparent quantum yield. Supplementary text 2. Method of calculation of Au clusters size 2R.

Acknowledgments

This work was supported by SABIC, the European Research Council through Advanced Grant ENERGYSURF (GT), EU COST Action CM1104, and the Royal Society (UK) through a Wolfson Research Merit Award to GT.

References

(1) Chen, M. S. & Goodman, D. W. Structure–activity relationships in supported Au catalysts. *Catal. Today* **2006,** *111***,** 22–33.

(2) Lai, X. & Goodman, D. W. Structure–reactivity correlations for oxide-supported metal catalysts: new perspectives from STM. *J. Mol. Catal.* **2000**, *162*, 33–50.

(3) Rodriguez, J. A., Senanayake, S. D., Stacchiola, D., Liu, P. & Hrbek, J. The Activation of Gold and the Water–Gas Shift Reaction: Insights from Studies with Model Catalysts. *Acc. Chem. Res.* **2014**, *47*, 773–782.

(4) Al-Azri, Z. H. N., Chan, A., Chen, W.-T., Ina, T., Idriss, H. & Waterhouse, G.I.N. The roles of metal co-catalysts and reaction media in photocatalytic hydrogen production: Performance evaluation of M/TiO_2 photocatalysts (M=Pd, Pt, Au) in different alcohol-water mixtures. *J. Catal.* **2015**, *329*, 355–367.

(5) M. Murdoch, G.W.N. Waterhouse, M.A. Nadeem, M.A. Keane, R.F. Howe, J. Llorca & H. Idriss. Photo-catalytic hydrogen production from ethanol over Au/TiO_2 anatase and rutile nanoparticles. Effect of Au particle size. *Nature Chemistry* **2011**, *3*, 489–492.

(6) Connelly, K. A. & Idriss, H. The photoreaction of TiO_2 and Au/TiO_2 single crystal and powder surfaces with organic adsorbates. Emphasis on hydrogen production from renewables. *Green Chem.* **2012**, *14*, 260–280.

(7) Majeed, I., Nadeem, M.M., Al-Oufi, M., Nadeem, M.A., Waterhouse, G.I.N., Badshah, A., Metson, J.B. & Idriss, H. On the role of metal particle size and surface coverage for photo-catalytic hydrogen production: A case study of the Au/CdS system. *App. Cata. B: Env.* **2016**, *182*, 266–276.

(8) Majeed, I.**,** Hussain, E., Nadeem M.M., Waterhouse, G.I.N., Badshah, A., Iqbal, A., Nadeem, M.A. & Idriss, H. On the Synergism between Cu and Ni for Photocatalytic Hydrogen Production and their Potential as Substitutes of Noble Metals. *ChemCatChem* **2016***, 8*, 3146–3155.

(9) Chen, W.-T., Chan, A., Sun-Waterhouse, D., Moriga, T., Idriss, H., & Waterhouse, G.I.N. Ni/TiO_2: A promising low-cost photocatalytic system for solar H_2 production from ethanol-water mixtures. *J. Catal.* **2015,** *326*, 43–53.

(10) Bamwenda, G.R., Tsubota, S., Nakamura, T., Haruta, M. Photoassisted hydrogen production from a water-ethanol solution: a comparison of activities of Au-TiO_2 and Pt-TiO_2, *Journal of Photochemistry and Photobiology A: Chemistry* **1995***, 89*, 177-189.

(11) Chen, T., Feng, Z., Wu, G., Shi, J., Ma, G., Ying,P., Li, C. Mechanistic Studies of Photocatalytic Reaction of Methanol for Hydrogen Production on Pt/TiO_2 by in situ Fourier Transform IR and Time-Resolved IR Spectroscopy. *J. Phys. Chem. C* **2007**, *111*, 8005-8014.

(12) Wang, K., Wei, Z., Ohtani, B., Kowalska, E. Interparticle electron transfer in methanol dehydrogenation on platinumloaded titania particles prepared from P25. *Catal. Today* **2018**, *303*, 327–333.

(13) Berr, M.J., Schweinberger, F.F., Döblinger, M., Sanwald, K.E., Wolff, C., Breimeier, J., Crampton, A.S., Ridge, C.J., Tschurl, M., Heiz, U., Jäckel, F., Feldmann, J. Size-Selected Subnanometer Cluster Catalysts on Semiconductor Nanocrystal Films for Atomic Scale Insight into Photocatalysis. *Nano Lett.* **2012**, *2*, 5903−5906.

(14) Valden, M., Lai, X. & Goodman, D. W. Onset of Catalytic Activity of Gold Clusters on Titania with the Appearance of Nonmetallic Properties. *Science* **1998***, 281*, 1647–1650.

(15) Haruta, M. Tsubota, S., Kobayashi, T., Kageyama, H., Genet, M.J., & Delmon, B. Low-Temperature Oxidation of CO over Gold Supported on TiO_2. α-Fe_2O_3, and Co_3O_4. *J. Catal.* **1993**, *144*, 175–192.

(16) Wu, T., Kaden, W. E., & Anderson, S. L. Water on Rutile TiO_2(110) and Au/TiO_2(110): Effects on Au Mobility and the Isotope Exchange Reaction. *J. Phys. Chem. C* **2008**, *112*, 9006–9015.

(17) Bowker, M., Bahruji, H., Kennedy, J., ones, W., Hartley, G., & Morton, C. The Photocatalytic Window: Photo-Reforming of Organics and Water Splitting for

Sustainable Hydrogen Production. *Catal. Lett.* **2015***, 145*, 214–219.

(18) Nadeem, M.A., Waterhouse, G.I.N., & Idriss, H. A study of ethanol reactions on O_2-treated Au/TiO_2. Effect of support and metal loading on reaction selectivity. *Surf. Sci.* **2016***, 650*, 40-50.

(19) Wahlström, E., Lopez N, Schaub R, Thostrup P, Rønnau A, Africh C, Laegsgaard E, Nørskov JK, & Besenbacher F. Bonding of Gold Nanoclusters to Oxygen Vacancies on Rutile TiO_2(110). *Phys. Rev. Lett.* **2003**, *90*, 37–4.

(20) Kolmakov, A. & Goodman, D. W. In situ scanning tunneling microscopy of oxide-supported metal clusters: Nucleation, growth, and thermal evolution of individual particles. *Chem. Record* **2002**, *2*, 446–457.

(21) Pang, C.L., Lindsay, R. & Thornton, G. Structure of clean and adsorbate-covered single-crystal rutile TiO_2 surfaces. *Chem. Rev.* **2013**, *113*, 3887-3948; and references therein.

(22) Kandiel, T., Ivanova, I., & Bahnemann, D. W., Long-term investigation of the photocatalytic hydrogen production on platinized TiO_2: an isotopic study. *Energy Environ. Sci*. **2014**, *7*,1420-1425.

(23) D. Matthey, D., Wang, J.G., Wendt, S., Matthiesen, J., Schaub, R., Lægsgaard, E., Hammer B., & Besenbacher, F., Enhanced Bonding of Gold Nanoparticles on Oxidized TiO_2(110). *Science* **2007**, 3*15*, 1692–1696.

(24) Jing Chung, H., Yurtsever, A., Sugimoto, Y., Abe, M. & Morita, S. Kelvin probe force microscopy characterization of TiO_2(110)-supported Au clusters. *Appl. Phys. Lett.* **2011**, *99*, 123102–4.

(25) Chen, D. A., Bartelt, M. C., Seutter, S. M. & McCarty, K. F. Small, uniform, and thermally stable silver particles on TiO_2(110)-(1 x 1). *Surf. Sci.* **200**0, *464*, L708–L714.

(26) Maeda, Y., Fujitani, T., Tsubota, S. & Haruta, M. Size and density of Au particles deposited on TiO_2(110)-(1 × 1) and cross-linked (1 × 2) surfaces. *Surf. Sci.* **2004**, *562*, 1–6.

(27) Mitchell, C. E. J., Howard, A., Carney, M. & Egdell, R. G. Direct observation of behaviour of Au nanoclusters on TiO_2(110) at elevated temperatures. *Surf. Sci.* **2001**, *490*, 196–210.

(28) Mellor, A., Humphrey, D., Yim, C. M., Pang, C. L., Idriss, H., & Thornton, G. Direct visualization of Au atoms bound to TiO_2(110) O-vacancies. *J. Phys. Chem. C* **2017**, *121*, 24721–24725.; and references therein.

(29) León, C. P., Sagisaka, K., Fujita, D. & Han, L. Ethanol adsorption on rutile TiO_2(110). *RSC Adv.* **2014**, *4***,** 8550–8558.

(30) Harrison, G., Katsiev, K., AlSalik, Y., Thornton, G, & Idriss, H. Switch in photocatalytic reaction selectivity: the effect of oxygen partial pressure on carbon-carbon bond dissociation over rutile TiO_2(110) single crystal. *J. Catalysis* **2018**, *363*, 117–127.

(31) Millard, L., Bowker, M. Photocatalytic water-gas shift reaction at ambient temperature. *J. Photochemistry and Photobiology A: Chemistry* **2002**, *148*, 91–95.

(32) Wenderich, K., Mul G. Methods, Mechanism, and Applications of Photodeposition in *Photocatalysis: A Review. Chem. Rev.* **2016**, *116*, 14587-14619.

(33) Wang, X.L., Wenqing Liu, W., Yu, Y.Y., Song, Y., Fang, W.Q., Daxiu Wei, D., Xue-Qing Gong, X-Q., Ye-Feng Yao, Y-F., Yang, G.H. Operando NMR spectroscopic analysis of proton transfer in heterogeneous photocatalytic reactions. *Nature Comm.* **2016**, *7*, 11918, 1-7.

(34) Migani, A., Blancafort, L., Excitonic Interfacial Proton-Coupled Electron Transfer Mechanism in the Photocatalytic Oxidation of Methanol to Formaldehyde on TiO_2(110). *J. Am. Chem. Soc.* **2016**, *138*, 16165−16173.

(35) Kershisa, M. D., White, M.G. Photooxidation of ethanol and 2-propanol on TiO_2(110): evidence for methyl radical ejection, *Phys. Chem. Chem. Phys.* **2013**, *15*, 17976—17982.

(36) Walenta, C.A., Kollmannsberger, S.L., Kiermaier, J., Winbauer, A., Tschurl, M, Heiz, U., Ethanol photocatalysis on rutile TiO_2(110): the role of defects and water. *Phys. Chem. Chem. Phys.*, **2015**, *17*, 22809—22814.

(37) Tan, S., Feng, H., Ji, Y., Zheng, Q., Shi, Y., Zhao, J., Zhao, A., Yang, J., Luo, Y., Bing, W., Hou, J.G., Visualizing Elementary Reactions of Methanol by Electrons and Holes on TiO_2(110) Surface. *J. Phys. Chem. C* **2018**, *122*, 28805−28814.

(38) Bo Wen, B., Yin, W-J., Selloni, A., Li-Min Liu, L.-M., Defects, Adsorbates, and Photoactivity of Rutile TiO_2 (110): Insight by First-Principles Calculations. *J. Phys. Chem. Lett.* **2018**, *9*, 5281−5287.

(39) Idriss, H. Ethanol Reactions over the Surfaces of Noble Metals/Cerium Oxide Catalysts *Platinum Metals Rev.* **2004**, *48*, 105-115.

(40) Jayaweera, P. M., Quah, E. L. & Idriss, H. Photoreaction of Ethanol on TiO_2(110) Single-Crystal Surface. *J. Phys. Chem. C* **2007**, *111*, 1764–1769.

(41) Ahmed, A.Y., Oekermann,T., Lindner, P. & Bahnemann, D., Comparison of the photoelectrochemical oxidation of methanol on rutile TiO_2 (001) and (100) single crystal faces studied by intensity modulated photocurrent spectroscopy. *Phys. Chem. Chem. Phys.* **2012**, *14*, 2774–2783

(42) Ahmed, A.Y., Kandiel, T. A., Lindner, P. & Bahnemann, Photocatalytic Activities of Different Well-defined Single Crystal TiO_2 Surfaces: Anatase versus Rutile, *J. Phys. Chem. Lett.* **2011**, *2*, 2461–2465.

(43) Furube, A., Asahi, T., Masuhara, H., Yamashita, H. & Anpo, M. Direct observation of a picosecond charge separation process in photoexcited platinum-loaded TiO_2 particles by femtosecond diffuse reflectance spectroscopy. *Chem. Phys. Lett.* **2001**, *336*, 424–430.

(44) Iwata, K., Takaya, T., Hiro-o Hamaguchi, H.-o, amakata, A., Taka-aki Ishibashi, T.-a, Hiroshi Onishi, H., & Kuroda, H. Carrier Dynamics in TiO_2 and Pt/TiO_2 Powders Observed by Femtosecond Time-Resolved Near-Infrared Spectroscopy at a Spectral Region of 0.9−1.5 μm with the Direct Absorption Method. *J. Phys. Chem. B* **2004**, *108***,** 20233–20239.

(45) Jovic, V., Smith, K. E., Idriss, H. & Waterhouse, G I.N. Heterojunction Synergies in Titania-Supported Gold Photocatalysts: Implications for Solar Hydrogen Production. *ChemSusChem* **2015**, *8*, 2551–2559.

(46) Bumajdad, A. & Madkour, M. Understanding the superior photocatalytic activity of noble metals modified titania under UV and visible light irradiation. *Phys. Chem. Chem. Phys.* **2014**, *16*, 7146–7158.

(47) Micic, O. I., Zhang, Y., Cromack, K. R., Trifunac, A. D. & Thurnauer, M. C. Photoinduced hole transfer from titanium dioxide to methanol molecules in aqueous solution studied by electron paramagnetic resonance. *J. Phys. Chem.* **1993**, *97*, 13284–13288.

(48) Yamakata, A., Ishibashi, T.-A. & Onishi, H. Electron- and Hole-Capture Reactions on Pt/TiO_2 Photocatalyst Exposed to Methanol Vapor Studied with Time-Resolved Infrared Absorption Spectroscopy. *J. Phys. Chem. B* **2002**, *106*, 9122–9125.

(49) Hansen, J. Ø., Bebensee, R., Martinez, U., Porsgaard, S., Lira, E., Wei, Y., Lammich, L., Li, Z., Idriss, H., Besenbacher, F., Hammer, B.,& Wendt, S. Unravelling Site-Specific Photo-Reactions of Ethanol on Rutile TiO_2(110). *Scientific Reports* **2016**, *6*, 21990 1 to 11 (2016)

(50) P. Maity, K. Katsiev, O. F. Mohammed & H. Idriss. Bulk Defect Mediated Photoexcited Charge Recombination in Anatase and Rutile TiO_2 Single Crystals. *J. Phys. Chem. C* **2018**, *122*, 8925–8932.

(51) Yamakata, A., Vequizo, J.J. M., & Matsunaga, H. Distinctive Behavior of Photogenerated Electrons and Holes in Anatase and Rutile TiO_2 Powders *J. Phys. Chem. C*, **2015**, *119*, 24538−24545.

(52) Jiang, Z., Zhang, W., Jin, L., Yang, X., Xu, F., Zhu, J., Huang, W., Direct XPS Evidence for Charge Transfer from a Reduced Rutile TiO_2(110) Surface to Au Clusters, *J. Phys. Chem. C* **2007***, 111*, 12434-12439.

(53) Reinecke, B. N., Kuhl, K. P., Ogasawara, H., Li, L., Voss, J., Abild-Pedersen, F., Nilsson, A., Jaramillo, T. F., Elucidating the electronic structure of supported gold nanoparticles and its relevance to catalysis by means of hard X-ray photoelectron spectroscopy, *Surf. Sci.* **2016**, *650*, 24-33.

(54) Chusuei, C. C., Lai, X., Luo, K., Goodman, D.W., Modeling heterogeneous catalysts: metal clusters on planar oxide supports, *Top. Catal.* **2001***,* 14, 71-83.

(55) Lee, S., Fan, C., Wu, T., Scott L., Anderson Agglomeration, support effects, and CO adsorption on Au/TiO_2(110) prepared by ion beam deposition, *Surf. Sci.* **2005**, *578*, 5-19.

(56) Khan, M.A., AlOufi, M., Maity, P., AlHowaish, I., H. Idriss, Investigation of the charge carrier dynamics in graphitic carbon nitride and their effect on photocatalytic hydrogen production. *J. Phys. Chem. C* **2018***, 122*, 16779–16787.

(57) Marcus, R. A. Electron transfer reactions in chemistry. Theory and experiment. *Rev. Mod. Phys.* **1993**, *65*, 1–12.

(58) Kamat, P.V., Quantum Dot Solar Cells. Semiconductor Nanocrystals as Light Harvesters, *J. Phys. Chem. C* **2008**, *112*, 18737-18753.

(59) Zhang, Z., Tang, W., Neurock, M., Yates, J.T. Jr., Electric charge of single Au atoms adsorbed on TiO_2(110) and associated band bending, *J. Phys. Chem. C* **2011**, *115*, 23848-23853.

(60) Hao, Q., Wang, Z., Wang, T., Ren, Z., Zhou, C., Yang X., Role of Pt Loading in the Photocatalytic Chemistry of Methanol on Rutile TiO_2(110), *ACS Catal*. **2019**, *9*, 286−294.

(61) Nesselberger, M., Roefzaad, M., Fayçal Hamou, R.F., Biedermann, P. U., Schweinberger, F.F., Kunz, S., Schloegl, K., Wiberg, G.K.H., Ashton, S., Heiz, U., Mayrhofer, K.J.J., Arenz, M., The effect of particle proximity on the oxygen reduction rate of size-selected platinum clusters, *Nat. Mat.* **2013**, *12*, 919-924.